Electronic Supplementary Information

Temperature dependence of the *anti*-CH_3CHOO reaction with water vapor

Liang-Chun Lin[1,2], Wen Chao[1,2], Chun-Hung Chang[1], Kaito Takahashi[1] and Jim Jr-Min Lin*[1,2]*

[1] Institute of Atomic and Molecular Sciences, Academia Sinica, No. 1, Sec. 4, Roosevelt Rd., Taipei 10617, Taiwan

[2] Department of Chemistry, National Taiwan University, No. 1, Sec. 4, Roosevelt Rd., Taipei 10617, Taiwan

AUTHOR INFORMATION

Corresponding Author

*kt@gate.sinica.edu.tw, jimlin@gate.sinica.edu.tw

Experimental Conditions

Flow and temperature control of the reactor

The kinetics measurement using the transient absorption was performed in a cylindrical glass tube (76 cm long, 2.0 cm inner diameter) with SiO_2 windows with anti-reflection coating. The carrier N_2 gas was mixed with water vapor, O_2 and CH_3CHI_2 in copper tubes at the upstream of this reactor. The water vapor was introduced into the mixture by flowing N_2 gas above a liquid water reservoir. For measurements at 308-328 K, the water reservoir was heated to be close to or slightly, ~5 K, higher than the reactor temperature to obtain higher water vapor concentration. The liquid CH_3CHI_2 was heated to ~307 K to obtain more stable vapor concentration. The concentrations of O_2, H_2O, and CH_3CHI_2 in the gas mixture were controlled with mass flow controllers (Brooks, 5850E or 5800E).

The reactor was placed in a temperature controlled water bath (Yih Der BL-730, stability ±0.1

K). We placed 3 resistance temperature detectors (RTDs, Newport Omega, F2020-1000-A) near the center and the two ends of the reactor. The gas mixture entered through the center of the reactor and exited through the two ends to a vacuum pump. Two small streams of N_2 gas, ~5% of the total flow, were used to purge the windows. The purge gas as well as the reactant gas mixture were passed through ~120 cm long copper tubes before entering the reactor. These tubes were also placed in the water bath for thermal equilibrium. We controlled the flow rate so that the gas in the reactor was fully refreshed between the 1 Hz photolysis pulses.

The [CH_3CHI_2] was measured upstream (before mixing it into the main gas mixture) by passing it through a small absorption cell and monitoring its absorption spectra using a deuterium lamp (Ocean Optics, D-2000) and a mini spectrometer (Ocean Optics, Maya 2000Pro). For experiment #1 (T = 288 K), to confirm that the precursor did not condense in the copper tube and contaminate our background signal, we directly measured the precursor absorption in the reactor by using a broad band plasma light source (Energetic, EQ-99) and another mini spectrometer (Ocean Optics, USB2000+UV-VIS-ES).

Table S1-A. Experimental conditions and results for the kinetic measurements of CH_3CHOO reaction with water vapor at 5 temperatures from 288 K to 328 K.

T/ K	Exp #	Laser fluence / mJ cm^{-2}	$P_{CH3CHI2}$ / mTorr	Max. Abs. of CI / 10^{-3}	P_{O2} / Torr	P_{Total} / Torr	k_{fast0} / sec^{-1}	# of data points
288	1-A	7.78	2.67	2.02	10.20	500.29	1689	20
	1-B	7.77	2.69	1.91	10.29	500.15	1522	22
298	2-A	7.82	2.72	1.80	10.25	500.15	1324	21
	2-B	7.42	2.74	1.72	10.16	500.40	1386	35
308	3-A	7.54	2.82	1.88	10.60	500.78	1310	24
	3-B	8.01	2.77	1.71	10.64	501.57	1229	18
318	4-A	8.90	2.62	1.68	10.70	501.70	1468	24
	4-B	7.88	2.87	1.68	10.50	500.25	1335	20
328	5-A	7.98	2.98	1.63	11.44	499.56	1282	14
	5-B	8.07	2.77	1.73	10.65	499.65	1574	14
	5-C	8.46	3.17	2.00	11.00	500.15	1764	32

Table S1-B. Experimental conditions and results for the kinetic measurements of CH_3CHOO reaction with water vapor at 4 total pressures from 100 Torr to 600 Torr at 298 K.

P_{cell} / Torr	Exp #	Laser fluence / mJ cm^{-2}	$P_{CH3CHI2}$ / mTorr	Max. Abs. of CI / 10^{-3}	P_{O2} / Torr	P_{Total} / Torr	k_{fast0} / sec^{-1}	# of data points
100	6-A	9.31	2.86	2.28	10.83	100.05	1421	20
	6-B	9.65	3.18	1.98	11.07	100.03	1342	22
	6-C	8.47	2.94	2.17	11.26	100.20	1414	27
	6-D	7.48	3.02	1.97	11.18	100.14	1285	19
200	7-A	8.86	2.86	2.29	10.94	200.02	1482	24
	7-B	9.01	2.78	2.13	10.50	200.04	1367	14
	7-C	7.03	2.89	1.72	10.87	200.48	1261	17
300	8-A	8.64	2.71	2.05	30.75	300.00	1308	31
	8-B	8.83	2.76	2.18	10.42	300.18	1319	25
	8-C	7.72	2.79	1.72	10.55	300.53	1369	31
600	9	7.08	2.50	1.47	9.91	600.28	1369	30

Table S1-C. Experimental conditions and results for the concentration dependent kinetic measurements of CH_3CHOO reaction with water vapor at 298 K.

Exp #	Laser fluence / mJ cm^{-2}	$P_{CH3CHI2}$ / mTorr	Max. Abs. of CI / 10^{-3}	P_{O2} / Torr	P_{Total} / Torr	k_{fast0} / sec^{-1}	# of data points
10-A	8.36	2.82	2.10	10.51	500.31	1620	18
10-B	4.08	2.68	1.22	10.59	500.19	1109	18

Error estimation for $[H_2O]$

We used a Rotronic sensor (Rotronic, HC2-S) to monitor the humidity and temperature of the gas mixture. The accuracy range for the sensor is 0.1-0.2 K temperature accuracy; 0.8% relative humidity accuracy at 298 K, 1.3% at 273 K and 313 K, 1.8% at 333 K, which leads to some uncertainty in $[H_2O]$. Since the water vapor pressure would change by 7% if the temperature is varied by 1 K, the 0.2 K uncertainty in the temperature would introduce an additional uncertainty of $0.2\times7\% = 1.4\%$ in $[H_2O]$.

To protect the Rotronic sensor from CH_3CHI_2 contamination, we placed it at upstream of the reactor which is prior to the mixing point of adding the CH_3CHI_2/N_2 sample gas (a small amount of

N_2 was used to carry CH_3CHI_2). Since the flow of CH_3CHI_2/N_2 was much smaller than that of the main gas mixture, the error in $[H_2O]$ introduced by this mixing is negligible (~0.01%).
By placing the Rotronic sensor as close as possible to the reactor, the precision and accuracy of $[H_2O]$ were mostly limited by the precision and accuracy of the sensor itself.

Transient absorption measurement

The transient absorption experiment is similar to those reported for CH_2OO.[1,2] We collimated the light from an excimer laser (Coherent, CompExPro 205, KrF 248 nm) with a cylindrical lens (f=1m) and collinearly passed it through the reactor by reflection from two ultra-steep long pass filters at 257 nm (Semrock, LP02-257RU-25). The average laser power was measured by a thermal pile power meter (Gentec EO, UP19K-30H-VM-D0) after passing through the reactor. The absorbance at 368 nm was detected using a 365 nm band pass filter (Edmund Optics, 65130, 10 nm, OD4) and a balanced photodiode detector (Thorlabs, PDB450A). The light from an LED light source (Hamamatsu, LC-L2 365 nm) was passed through the reactor 8 times to enhance the absorption signal. To account for the fluctuation in the light source intensity, we simultaneously measured the reference signal originating from the light source without passing it through the reactor and subtracted it from the absorption signal. The photodiode output was recorded with a digital oscilloscope (LeCroy, HDO4034), and averaged for 120 laser pulses. In Figure S1, we present the raw data as well as the background for the time trace. By subtracting the background for the raw signal given in Figure S1(a), we obtain the signal given in Figure 1 of the main text. In Figure S1(b), we present the early time trace.

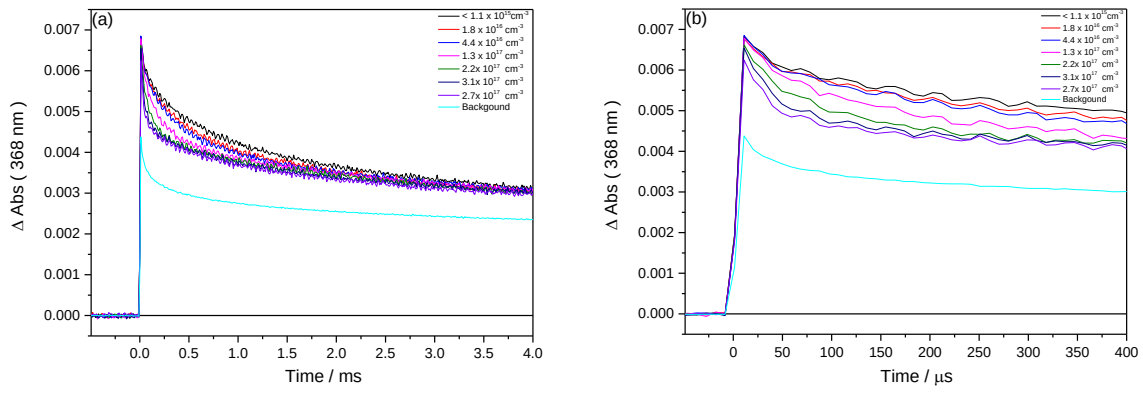

Figure S1. Raw time trace of transient absorption at 368 nm as well as the background (a) for the first 4 ms and (b) for the first 400 μs. These results are for the 288 K given in Figure 1 of the main text.

Details concerning the fitting

In the following we present the details for the fitting procedure of the transient absorption signal. We will use the double exponential function

$$\Delta Abs(t) = C_{\text{offset}} + C_{\text{slow}} e^{-t/\tau_{\text{slow}}} + C_{\text{fast}} e^{-t/\tau_{\text{fast}}}, \quad (1)$$

and due to the difference in time scales of τ_{fast} and τ_{slow}, we first fit the slow contribution using the long-time data. Due to the CH_3CHOO formation kinetics ($CH_3CHI_2 + h\nu \rightarrow CH_3CHI + I$, $CH_3CHI + O_2 \rightarrow CH_3CHOO + I$) and background interference from the photolysis laser, we ignore the data for the first 8 μs (t_0 = 8 μs). We define the long-time data as the signal from $t_0 + 4\tau_{\text{fast}}$ to 6 ms, where τ_{fast} is the lifetime of the fast component. For the first iteration we use the water concentration and our previous theoretical bimolecular rate coefficients[3] for the *anti*-CH_3CHOO water monomer/dimer reaction ($k_{\text{m,anti}}/k_{\text{d,anti}}$) to estimate

$$\tau_{\text{fast}} = \frac{1}{k_{\text{d,anti}}(T)[(H_2O)_2] + k_{\text{m,anti}}(T)[H_2O]}. \quad (2)$$

We fit the long-time data to

$$C_{\text{offset}} + C_{\text{slow}} e^{-t/\tau_{\text{slow}}}. \quad (3)$$

Here, we used the following initial conditions: the minimum value in the data was used for C_{offset}, while the difference between the maximum and minimum values in the data was used for C_{slow}, and for τ_{slow} we used equation (2) above with the theoretical bimolecular rate coefficients for the *syn*-CH_3CHOO water monomer and dimer reactions reported previously[3]. The obtained fit can be seen as the blue line in Figure S2.

After obtaining the best fit value for $C_{\text{offset}}, C_{\text{slow}}, \tau_{\text{slow}}$ we define the short-time data by subtracting equation (3) from the original data for the time between t_0 to $t_0 + 4\tau_{\text{fast}}$. Then we fit these data to

$$C_{\text{fast}} e^{-t/\tau_{\text{fast}}}. \quad (4)$$

Here we used the following for the initial conditions: the difference between the maximum and minimum values in the data for C_{fast} and equation (2) for τ_{fast}. This can be seen as the magenta line in Figure S2. After obtaining all 5 parameters for equation (1), we repeat the fitting procedure for the long- and short-time data until convergence is reached after ~5 iterations. The green line is the summation of the fast decay and the slow decay.

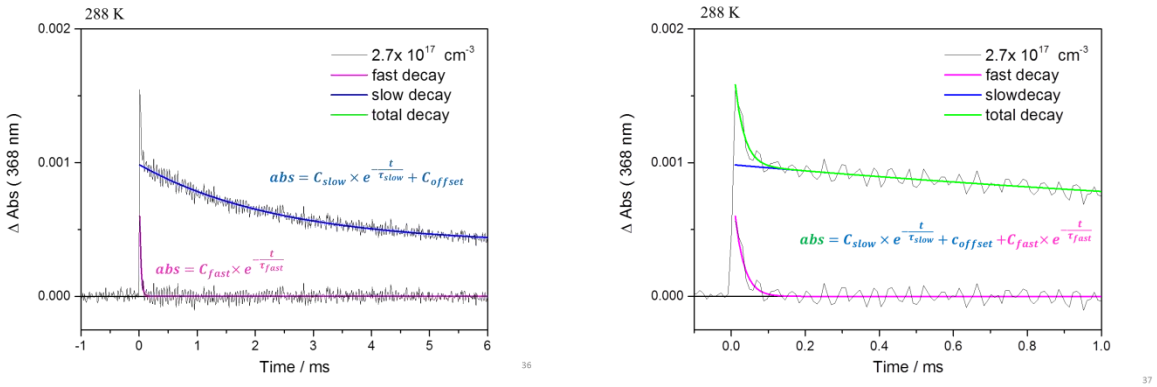

Figure S2. Fitting procedure for high water concentration ([H_2O]=2.7×10^{17} cm^{-3}) at 288 K.

After performing the fitting with the aforementioned procedure, as given in Figure S3, we noticed a jump in the $C_{\text{slow}}, C_{\text{fast}}$ at low humidity. This is because our assumption that the decay of *anti*-CH_3CHOO is much faster than the decay of *syn*-CH_3CHOO is not satisfied at low humidity. To remedy this issue, we assumed a linear dependence of the $C_{\text{offset}}, C_{\text{slow}}, C_{\text{fast}}$ on [H_2O]. Then we obtain a linear fit for the high humidity results (RH =20-80%) as given by the lines in Figure S3. Lastly, we performed the nonlinear fitting for the low humidity (RH $\leq$ 20%) data with a constraint that the values of $C_{\text{offset}}, C_{\text{slow}}, C_{\text{fast}}$ are within 9×10^{-5} apart from the values obtained from the linear fit. After constraining the C_{slow}, C_{fast} with the linear fit, we performed the sequential fitting mentioned above with the revised $C_{\text{slow}}, C_{\text{fast}}$. We then placed these five parameters as the initial condition to the double exponential function to fit the time traces from t_0 to 6 ms, and repeated the fitting until convergence was reached.

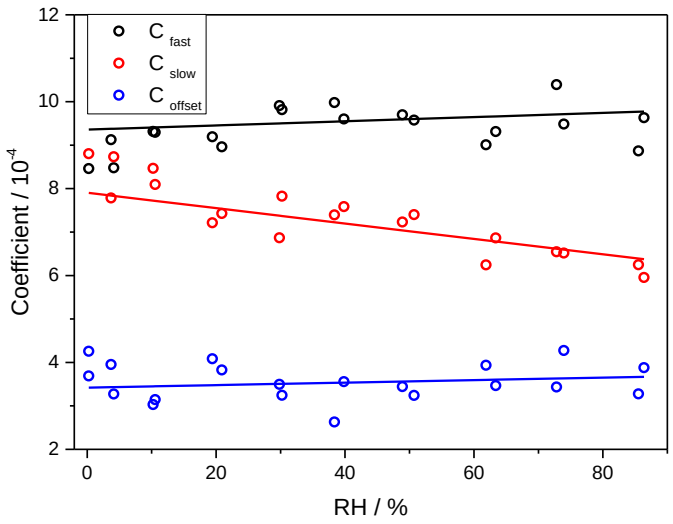

Figure S3. The relative humidity dependence of $C_{\text{fast}}, C_{\text{slow}}, C_{\text{offset}}$ and linear fit as a function of relative humidity for 288 K experiment #1-A.

Here we will discuss the variances in the coefficients $C_{\text{fast}}, C_{\text{slow}}, C_{\text{offset}}$ as a function of laser fluence, pressure, and temperature. As shown in Figure S4, the absolute values of C_{fast} and C_{slow} at 298 K show laser fluence dependence. However the ratio between the two coefficients are similar to each other. Furthermore, when we compare the ratio between C_{fast} and C_{slow} at 298 K obtained at 100 and 500 Torr total pressures, we also see very small variations. On the other hand, if we compare the results at different temperatures, we can notice that the relative contribution of C_{fast} increased at higher temperatures. As conclusion, ratios between C_{fast} and C_{slow} show small laser fluence and pressure dependence, but show slightly positive temperature dependence.

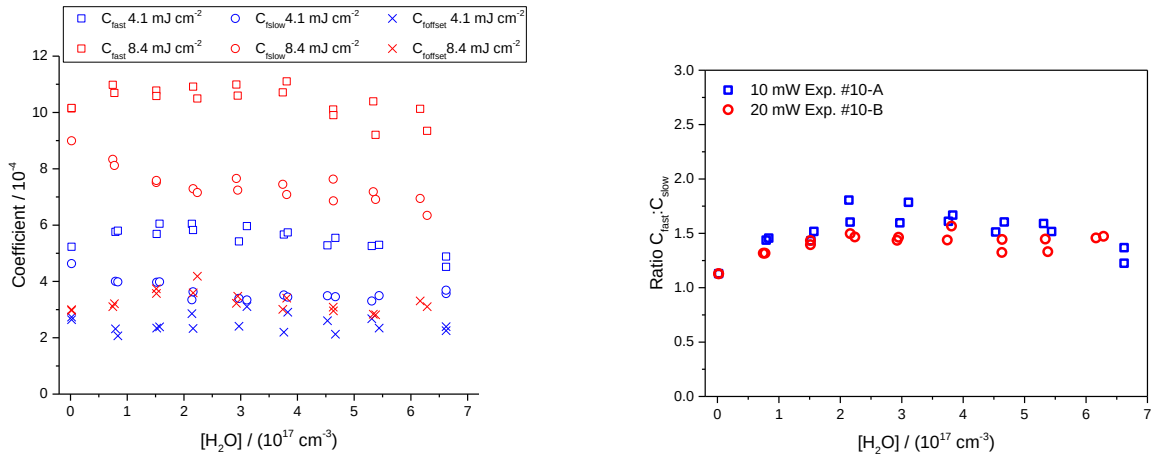

Figure S4. The water concentration dependence of $C_{\text{fast}}, C_{\text{slow}}, C_{\text{offset}}$ obtained at 298 K using 4.1 and 8.4 mJ cm^{-2} laser fluences. The ratio between C_{fast} and C_{slow} are given on the left hand plot.

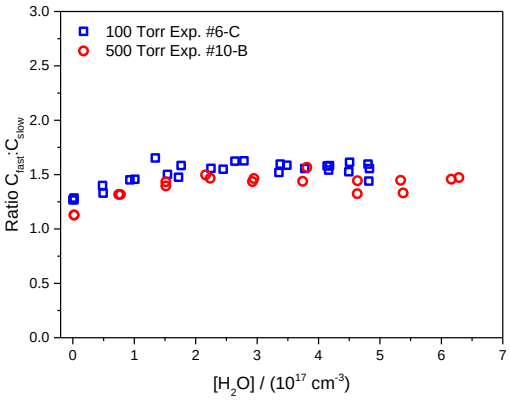

Figure S5. The water concentration dependence of the ratio between C_{fast} and C_{slow} obtained at 298 K for 100 and 500 Torr.

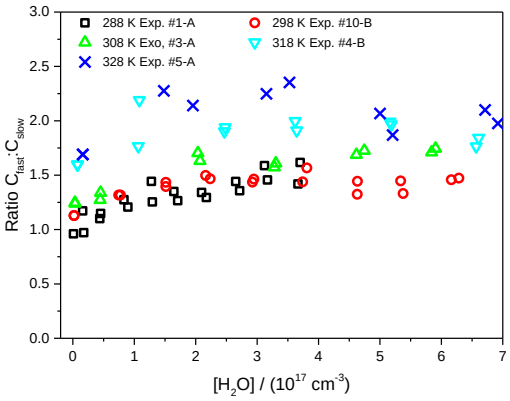

Figure S6. The water concentration dependence of the ratio between C_{fast} and C_{slow} obtained at 288, 298, 308, 318, and 328 K

After obtaining $k_{\text{fast}} = \frac{1}{\tau_{\text{fast}}}$ from the nonlinear fitting, we subtracted the rate for the dry condition and plotted the effective first-order rate k_w as a function of water concentration and temperature. In Figure S7 we present our effective rate as well as the fitted surface using the water dimerization equilibrium constant $K_{eq} = [(H_2O)_2]/[H_2O]^2$ given by Ruscic.[4]

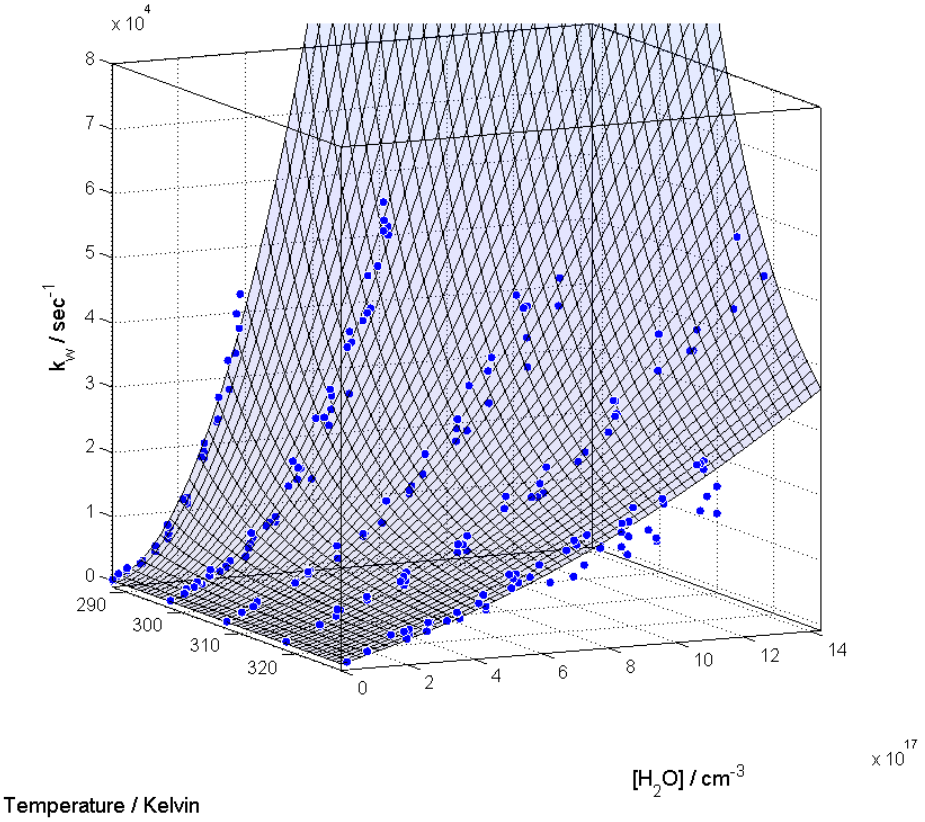

Figure S7. The first order effective rate k_w for *anti*-CH_3CHOO + water vapor reaction as a function

of water concentration and temperature. The surface obtained from the Arrhenius equation fit is also presented.

Figures S8-A-E are the cuts from Figure S4 at five temperatures along with the partition between water dimer and water monomer contributions at different water concentration.

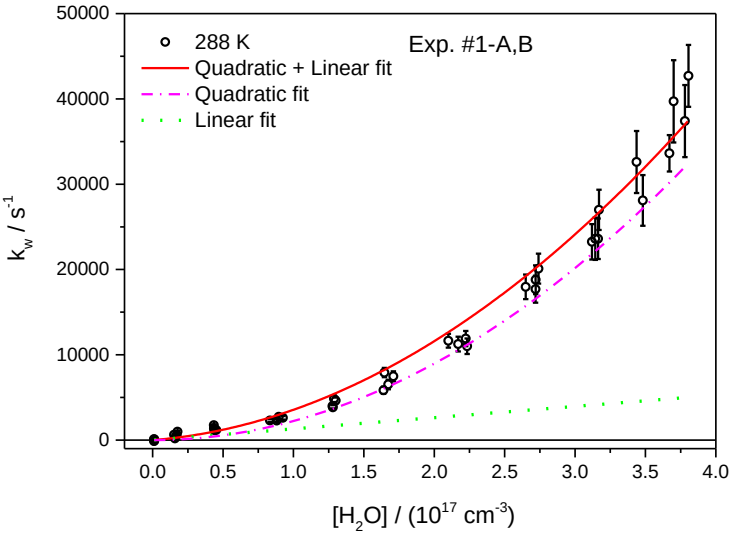

Figure S8-A. The water concentration dependence of k_w for the *anti*-CH_3CHOO + water vapor reaction at 288 K. The linear fit represents water monomer contribution (green dotted line), and the quadratic fit represents water dimer contribution (magenta dot-dash line).

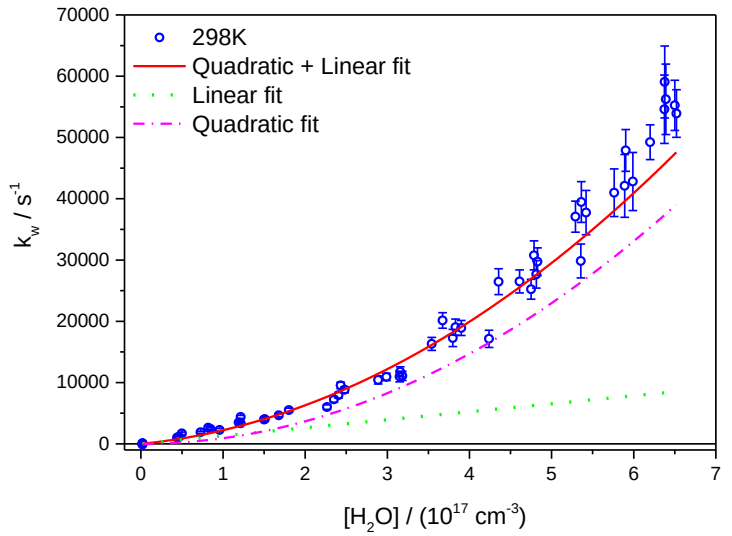

Figure S8-B. The water concentration dependence of k_w for the *anti*-CH_3CHOO + water vapor reaction at 298 K.

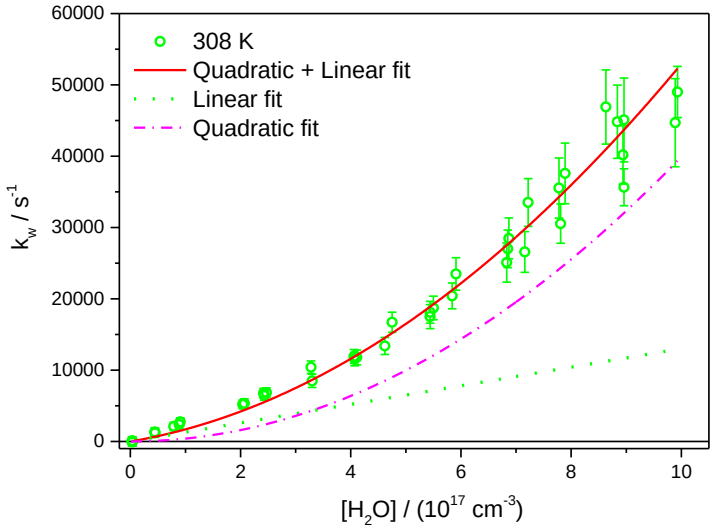

Figure S8-C. The water concentration dependence of k_w for the *anti*-CH_3CHOO + water vapor reaction at 308 K.

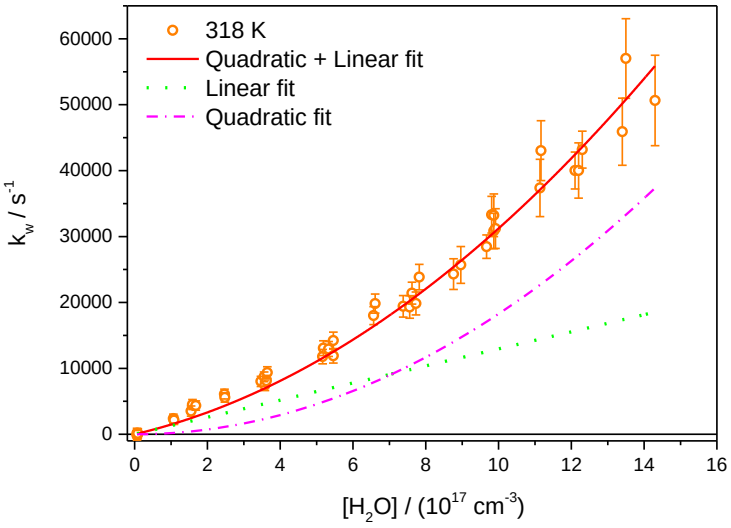

Figure S8-D. The water concentration dependence of k_w for the *anti*-CH_3CHOO + water vapor reaction at 318 K.

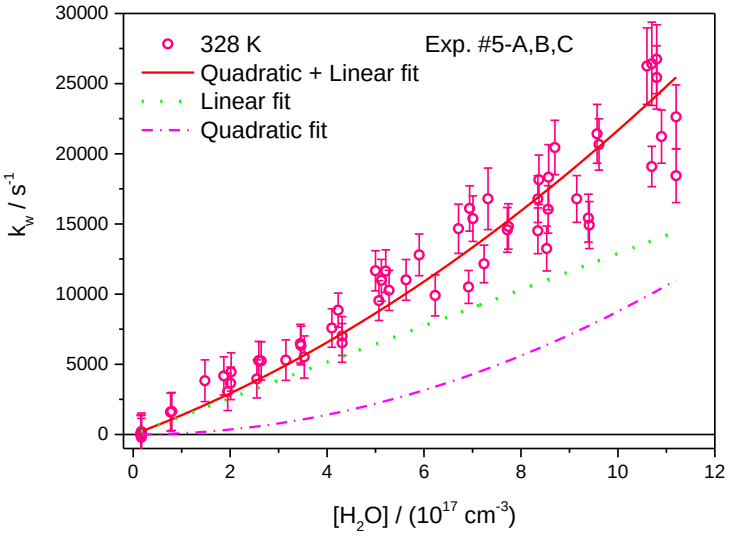

Figure S8-E. The water concentration dependence of k_w for the *anti*-CH_3CHOO + water vapor reaction at 328 K.

As can be seen in Figure S8-B, water dimer contribution cannot be ignored at $[H_2O] > 3\times10^{16}$ cm^{-3}, therefore one must consider the dimer contribution at greater water concentrations. In Figure S9 below, we compare our room temperature effective rate coefficients with those obtained by Sheps et al.[5]

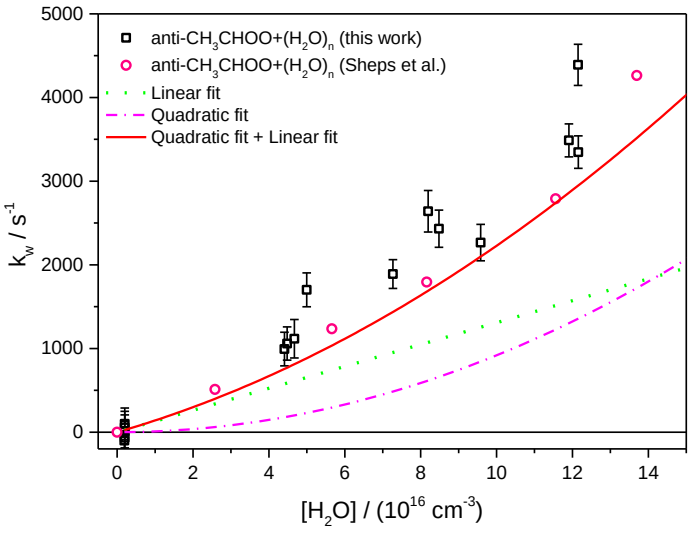

Figure S9. The water concentration dependence of k_w for the *anti*-CH_3CHOO + water vapor reaction at 298 K for $[H_2O] \leq 14\times10^{16}cm^{-3}$. The linear fit represents water monomer contribution (green dotted line), and the quadratic fit represents water dimer contribution (magenta dot-dash line). The black squares with error bars are from this work; the pink circles are from Sheps et al.[5]

As mentioned in the text, one can also perform a fit to

$$k_{w=}k_d K_{eq}[H_2O]^2 + k_m[H_2O]$$

independently at each temperature. In Table S2, we compare the results obtained from our global fit given in Figure S4 to the results obtained from independent fits at each temperature. We note that at low temperatures the dimer contribution dominates and we were not able to obtain the monomer rate coefficients, while at the highest temperature, we could not obtain the dimer rate coefficient. By using a global fit, we obtain a balanced fit between the water monomer and dimer contributions.

Table S2. Temperature dependence of the bimolecular rate coefficient for *anti*-CH_3CHOO reaction with water monomer (k_m) and with water dimer (k_d) from the two methods: the global fit method and the independent fit at each temperature.

T (K)	Global fit		Independent fit	
	k_d (10^{-11} cm^3 sec^{-1})	k_m (10^{-14} cm^3 sec^{-1})	k_d (10^{-11} cm^3 sec^{-1})	k_m (10^{-14} cm^3 sec^{-1})
288	8.98±0.70	1.32±0.35	10±1.0	
298	4.40±0.29	1.31±0.26	5.9±0.3	
308	2.26±0.16	1.30±0.18	1.9±0.7	1.7±0.7
318	1.21±0.11	1.30±0.14	1.0±0.3	1.7±0.6
328	0.67±0.08	1.29±0.14		2.0±0.2

Pressure dependence

The values for the pressure dependent rate coefficients for the *anti*-CH_3CHOO water dimer reaction at 298 K are given in Table S3.

Table S3. The pressure dependence of the *anti*-CH_3CHOO and water dimer rate coefficient at 298 K, assuming that the rate coefficient of *anti*-CH_3CHOO reaction with water monomer is pressure independent ($k_m = 1.31\times10^{-14}$cm^{3}s^{-1}).

Pressure (Torr)	k_d (cm^{3}s^{-1})
100	$3.73\pm0.13\times10^{-11}$
200	$3.90\pm0.13\times10^{-11}$
300	$4.29\pm0.09\times10^{-11}$
500	$5.05\pm0.17\times10^{-11}$
600	$4.89\pm0.26\times10^{-11}$

Laser fluence dependence

In experiments 10-A and 10-B, we performed the experiment at lower CH_3CHOO concentration by reducing the 248 nm laser fluence by half. As shown in Figure S10 below, this does not affect the effective rate of the water reaction.

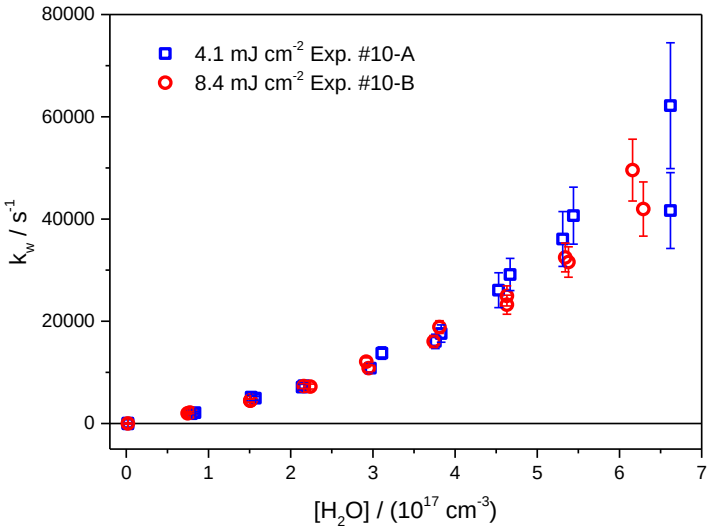

Figure S10. The water concentration dependence of k_w for the *anti*-CH_3CHOO + water vapor reaction at 298 K using different laser fluence.

anti-CH_3CHOO versus CH_2OO bimolecular rate coefficients

In Figure S11, we present the dimer contribution R_d to the total rate calculated using the Arrhenius fit to our theoretical rate coefficients reported previously.[3] As can be seen from the plot for *anti*-CH_3CHOO, theoretical simulation predicts that water monomer reaction will dominate at atmospherically relevant temperature and humidity. This is quite different from the experimental result given in Figure 6 of the main text.

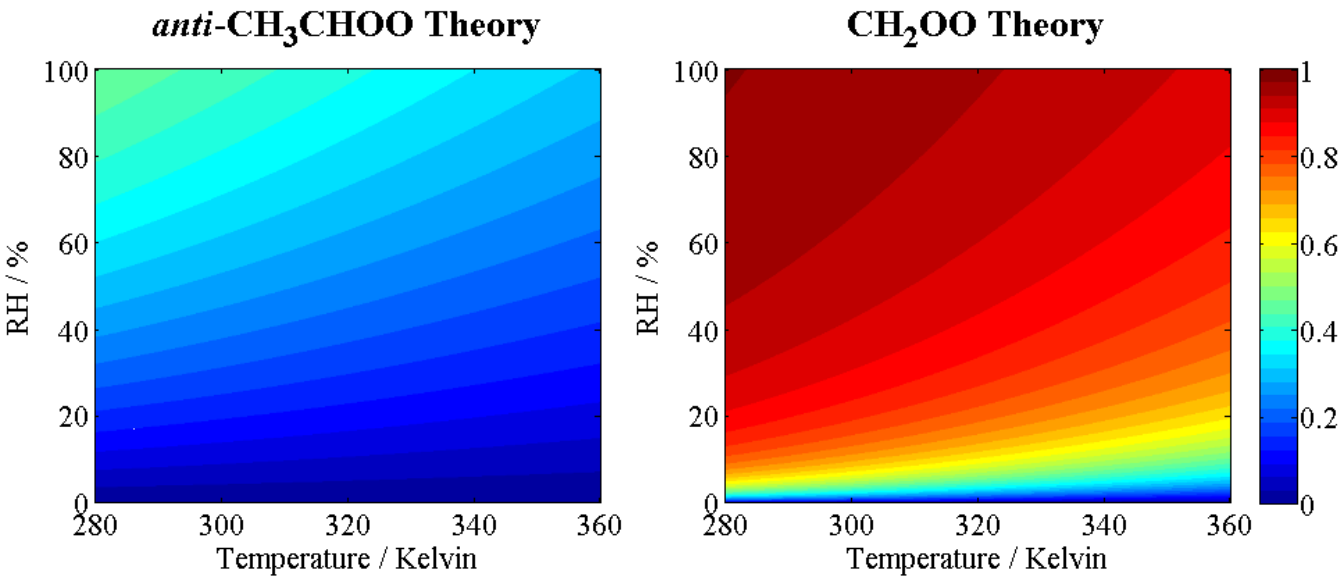

Figure S11. The relative humidity and temperature dependence of the water dimer contribution to the water vapor rate obtained from theoretical bimolecular rate coefficients.

Reference

1 W. Chao, J. Hsieh, C. Chang and J. J. Lin, *Science*, 2015, **347**, 751–754.

2 M. C. Smith, C.-H. Chang, W. Chao, L.-C. Lin, K. Takahashi, K. A. Boering and J. J.-M. Lin, *J. Phys. Chem. Lett.*, 2015, **6**, 2708–2713.

3 L.-C. Lin, C.-H. Chang, W. Chao, M. C. Smith, C.-H. Chang, J. J. Lin and K. Takahashi, *Phys. Chem. Chem. Phys.*, 2016, **18**, 4557–4568.

4 B. Ruscic, *J. Phys. Chem. A*, 2013, **117**, 11940–11953.

5 L. Sheps, A. M. Scully and K. Au, *Phys. Chem. Chem. Phys.*, 2014, **16**, 26701–26706.